Journal of Sound and Vibration 328 (2009) 9–28

Contents lists available at ScienceDirect

Journal of Sound and Vibration

journal homepage: www.elsevier.com/locate/jsvi

Controlling friction-induced instability by recursive time-delayed acceleration feedback

S. Chatterjee *, P. Mahata

Department of Mechanical Engineering, Bengal Engineering and Science University, Shibpur, Howrah, West Bengal 711 103, India

ARTICLE INFO

Article history:
Received 31 October 2008
Received in revised form
3 June 2009
Accepted 28 July 2009
Handling Editor: J. Lam
Available online 3 September 2009

ABSTRACT

A novel time-delayed acceleration feedback method of controlling friction-induced instability is proposed. A single degree-of-freedom mechanical oscillator on a moving belt represents the basic friction-driven system. The control force is synthesized based on an infinite weighted sum of the acceleration of the vibrating mass measured at regular intervals in the past. Such a control force can be effectively produced by the recursive summation of the time-delayed acceleration and the time-delayed control signal, and hence the technique is termed as the recursive time-delayed acceleration feedback control. The local stability analysis of the equilibrium reveals nontrivial and beneficial influences of the recursive gain on the system performance. Robustness of the control is shown to improve with the increasing value of the recursive gain. A multiple time scale based analysis of the system elucidates the role of the recursive gain in enhancing the amount of dissipation produced by the control action. The influences of the time-delay and the control gain on the optimized performance of the system are also discussed. Numerical simulations of the system equations corroborate the analytical results. The present method is believed to be applicable to any self-excited system having a large degree of instability that is not removable by an ordinary time-delayed feedback.

1. Introduction

Friction-induced self-excited vibration is a common phenomenon in mechanical and electromechanical systems. In most systems, friction-induced vibrations are highly undesirable. For example, self-excited vibration in mechanical brakes causes noise related discomfort. Another example is the controlled positioning systems that have now become an integral part of a large number of industrial production systems as well as consumer electronics products. Friction often causes high level of positioning inaccuracies by inducing self-excited oscillations around the desired position. Thus, it is not surprising that researchers, over the past few years, have put serious efforts towards understanding the phenomena and finding suitable means of controlling such unwanted oscillations.

Researchers have identified three major mechanisms of friction-driven oscillations. The most common reason of the friction-induced instability is attributed to the velocity-weakening characteristics of the friction force, which is also known as the Stribeck effect. Other widely studied mechanisms are mode-coupling and sprag-slip instabilities. Elaborate and seminal reviews of the previous research on this topic are available in [1,2].

* Corresponding author.
E-mail address: shy@mech.becs.ac.in (S. Chatterjee).

0022-460X/$ - see front matter © 2009 Elsevier Ltd. All rights reserved.
doi:10.1016/j.jsv.2009.07.028

Literature on controlling friction-induced vibrations is vast. Various active and passive methods of controlling friction-induced oscillations are proposed in the literature [3–8]. Various methods including dynamic vibration absorbers, linear and nonlinear control of the tangential and the normal forces and high-frequency excitations, etc. are discussed. In recent times, many researchers have investigated active control of vibrations using time-delayed state (full or partial) feedback [9–12]. Atay [13,14], Maccari [15–17] and Li et al. [18] discuss the use of time-delayed state feedback method in controlling free, forced and parametric vibrations of the Van der Pol oscillator. Studies on the use of time-delayed feedback in controlling friction-induced instabilities and oscillations are rather limited. Elmer [19] proposes a method of controlling friction-induced oscillations by normal load modulation based on the time-delayed state feedback. His method is very similar to that proposed by Pyragas [20]. Das and Mallik [21] consider the time-delayed PD feedback control of the forced vibration of a friction-driven system. Here, control force acts in the slipping direction. Refs. [19,21] consider only the Stribeck type instability. Chatterjee [22] has discussed the Pyragas type [20] time-delayed feedback control of different types of friction-induced instabilities, namely (1) Stribeck instability governed by velocity-weakening characteristics of friction force, (2) mode-coupling instability, and (3) sprag-slip instability. Recently, Chatterjee and Mahata [23] have explored the efficacy of a time-delayed vibration absorber for controlling the Stribeck instability and the associated self-excited oscillation of a friction-driven system.

The present paper deals with the efficacy of a recursive time-delayed controller in suppressing the self-excited vibration of a mechanical oscillator driven by the velocity-weakening friction force. A spring supported mass on a moving belt represents an archetypal model of the friction-driven self-excited system. The control force is considered to act directly on the vibrating mass in the direction of slipping. The control signal, in the proposed strategy, is determined by an infinite, weighted sum of the acceleration of the vibrating system measured at regular time intervals in the past. The basic idea is adapted from the concept of *extended time-delay auto synchronization* (ETDAS) control strategy originally proposed by Socolar et al. [24] for stabilizing the unstable periodic orbits embedded in a chaotic attractor. However, the full potential of this class of control strategy in mitigating resonant vibrations of flexible mechanical and structural components have been recently explored by Chatterjee [25]. Because the control signal can also be determined recursively by the weighted sum of the time-delayed acceleration and the time-delayed control signal, the proposed strategy is pertinently called hereafter as the *recursive time-delayed feedback control* (RTDFC). A mathematical model of the system is developed. The local stability of the equilibrium of the system is studied based on the linearized model around the equilibrium. The dissipative effects of the recursive feedback are analyzed using the multiple time scale method. Robustness of the stability is also discussed. Formulae for the maximum dissipation and robustness of the control are derived. The characteristic behaviour of the system is explained in light of the dominant poles of the system. Direct numerical simulations of the mathematical model of the system substantiate the theoretical results.

2. Mathematical model

A model of the controlled system is depicted in Fig. 1. The elastic member is represented by a single dof mechanical oscillator where the mass (M) is suspended by a spring of stiffness K from a fixed support. The mass is placed upon a belt that is moving with a constant velocity V_b. The control force (F_c) and the friction force (F) are acting along the direction of slipping. Although some structural damping, however small, is present in any structural system, its effect can be neglected in the mathematical modeling when the primary objective is to analyze the stabilizing effect of the control on the system dynamics because structural damping always improves the stability condition. If X is the displacement of the mass at any instant of time t, then the equation of motion of the system reads as

$$M\ddot{X} + KX = F(V_b - \dot{X}) + F_c, \tag{1}$$

where the 'overdot' denotes differentiation with respect to the time variable t.

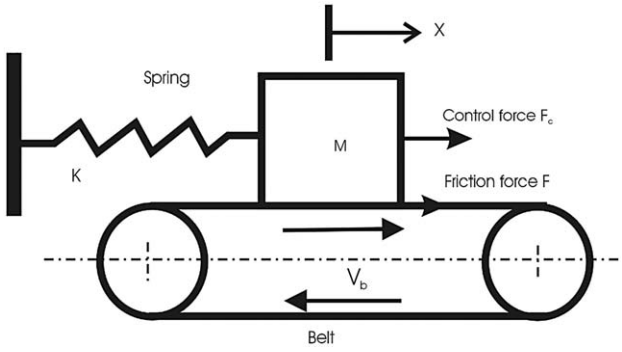

Fig. 1. Mathematical model of the controlled system.

The friction force (F) between the primary mass and the belt is considered to follow a velocity-weakening characteristic best illustrated in Fig. 2. Various functional forms have been proposed in the literature for mathematically expressing this typical velocity dependence of the friction force. The polynomial representation with up to third order term is mathematically more amenable and widely used in the literature. However the present paper considers, an exponential model of the velocity-weakening friction characteristic as proposed by Hinrichs et al. [26]. The exponential model, in comparison to the polynomial model, goes a long way in explaining the experimentally observed complex dynamics arising in many friction-driven systems [27]. The exponential model of the friction force used here is expressed as

$$F(v) = c^* v + N_0(\mu + \Delta\mu e^{-a^*|v|}) \tanh(\beta^* v), \tag{2}$$

where v (here $v = V_b - \dot{X}$) is the relative sliding velocity and c^* is the viscous component of the friction force. μ is the minimum kinetic friction coefficient and $\Delta\mu$ is the difference between the static friction coefficient and the minimum kinetic friction coefficient. N_0 is the normal load and a^* is a model parameter that determines the slope of the friction-velocity curve in the low velocity range. $\tanh(\beta^* v)$ is the continuous functional representation of signum function with $\beta^* \gg 1$.

The control force F_c is given by

$$F_c = K_c U, \tag{3}$$

where K_c is the control gain and U is the control signal. The control law is formulated as the infinite weighted sum of the acceleration of the mass measured at equal time intervals in the past and is mathematically expressed as

$$U(t) = \sum_{n=1}^{\infty} R^{n-1} \ddot{X}(t - nT^*). \tag{4}$$

Here, T^* is the minimum time-delay and R is a real parameter termed as the recursive gain. The value of R is in the range of -1 to $+1$. It is noteworthy that $R = 0$ corresponds to an ordinary time-delayed feedback. As mentioned earlier, the control law is adapted from the concept of ETDAS [24] and the control signal given by Eq. (4) can be viewed as a special form of multiple time-delayed feedback with infinite number of commensurate time-delays having monotonically decreasing weight. However, this particular form with infinite number of terms poses problem in the physical implementation of the control. Fortunately, an alternative recursive representation of the control signal U exists as shown below

$$U(t) = \ddot{X}(t - T^*) + RU(t - T^*). \tag{5}$$

The above recursive form renders the control law physically realizable. The control signal having the recursive form can be interpreted as the weighted sum of the time-delayed acceleration and the control signal itself. It may also be noted that the control force becomes trivial after the equilibrium is stabilized.

Eqs. (1)–(5) can be recast in the following non-dimensional form:

$$\ddot{y} + y = f(v_0 - \dot{y}) + f_c, \tag{6}$$

where

$$x_0 = \frac{N_0}{M\omega_n^2}, \quad y = \frac{X}{x_0}, \quad v_0 = \frac{V_b}{\omega_n x_0}, \quad \omega_0 = \sqrt{\frac{K}{M}}$$

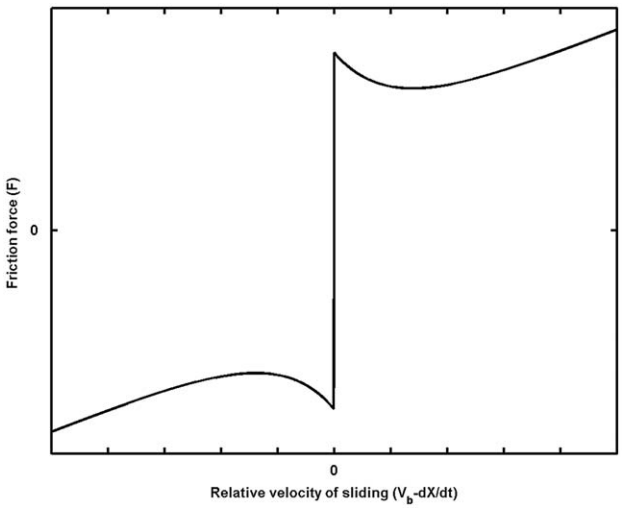

Fig. 2. Typical velocity-weakening friction characteristic.

are the non-dimensional quantities and the 'overdot' denotes differentiation with respect to the non-dimensional time $\tau = \omega_0 t$.

The non-dimensional control force f_c is expressed as:

$$f_c = k_c u^*, \tag{7}$$

where $k_c = K_c/M\omega_n^2$ is the non-dimensional control gain and the non-dimensional representation of the control is

$$u^*(\tau) = \sum_{n=1}^{\infty} R^{n-1}\ddot{y}(\tau - nT) = \ddot{y}(\tau - T) + Ru^*(\tau - T), \tag{8}$$

where $T = \omega_n T^*$ is the non-dimensional time-delay.

The non-dimensional friction force f is given as

$$f = c(v_0 - \dot{y}) + (\mu + \Delta\mu e^{-a|v_0 - \dot{y}|}) \tanh(\beta(v_0 - \dot{y})), \tag{9}$$

where $c = c^*/M\omega_n$, $a = a^*\omega_n x_0$, $\beta = \beta^*\omega_n x_0$ are the non-dimensional quantities.

3. Local stability analysis

Detailed stability analysis of the uncontrolled system is available in the literature [4,5,7] and therefore, is avoided here. It is known that the static equilibrium of the uncontrolled system is unstable, particularly for very low velocities of sliding. In this section, the local stability of the equilibrium of the controlled system is analyzed. Towards this end, it is pertinent to assume that the system is vibrating near the equilibrium position. In other words, the mass is always slipping on the belt; this is possible when the magnitude of the velocity of the mass is always less than the belt velocity i.e., $|\dot{y}| < v_0$. Thus, the reversal of the relative velocity of slipping and hence the condition of the stick-slip vibration is precluded.

Substituting $\ddot{y} = \dot{y} = 0$ into Eq. (6) and noting that the control force f_c vanishes at the equilibrium, the equilibrium position of the mass is obtained as

$$y_{eq} = \mu + \Delta\mu e^{-av_0} + cv_0. \tag{10}$$

As v_0 is always greater than $|\dot{y}|$ and $\beta \gg 1$, the argument of the hyperbolic function in Eq. (9) is a large positive quantity and thus, the hyperbolic term can be closely approximated as unity.

Using the coordinate transformation $z = y - y_{eq}$, Eqs. (6)–(9) can be recast in the following form:

$$\ddot{z} + z = \gamma(e^{a\dot{z}} - 1) - c\dot{z} + k_c u, \tag{11}$$

where $\gamma = \Delta\mu e^{-av_0}$.

Note that the equilibrium of the system given by Eq. (11) is at (0,0). The control signal u is now expressed as

$$u(\tau) = \sum_{n=1}^{\infty} R^{n-1}\ddot{z}(\tau - nT). \tag{12}$$

The recursive forms of the above control signals are now rewritten as

$$u(\tau) = \ddot{z}(\tau - T) + Ru(\tau - T). \tag{13}$$

The above expression is particularly useful for real-time implementation of the proposed control strategy.

Expanding the nonlinear term in Eq. (11) in the Taylor series and neglecting the higher order terms, one finally obtains the following linearized equation of motion:

$$\ddot{z} - c_e\dot{z} + z = k_c u, \tag{14}$$

where $c_e = \gamma a - c$.

Taking the Laplace transform on both sides of Eqs. (13) and (14), yields the following characteristic equation:

$$P(s) - Q(s)\, e^{-sT} = 0, \tag{15}$$

where $P(s) = s^2 - c_e s + 1$, and $Q(s) = Ls^2 - c_e Rs + R$, with $L = R + k_c$.

The roots of the characteristic equation (Eq. (15)) determine the stability of the equilibrium of the system. On a switching boundary, Eq. (15) has a pair of purely imaginary roots. Substituting $s = j\omega$ into Eq. (15) and separating the real and imaginary parts, one obtains

$$\begin{bmatrix} A_{11} & A_{12} \\ A_{21} & A_{22} \end{bmatrix} \begin{Bmatrix} \cos\omega T \\ \sin\omega T \end{Bmatrix} = \begin{Bmatrix} B_1 \\ B_2 \end{Bmatrix}, \tag{16a,b}$$

where $A_{11} = A_{22} = L\omega^2 - R$, $A_{12} = -A_{21} = c_e R\omega$, $B_1 = \omega^2 - 1$ and $B_2 = -c_e\omega$

Now, Eq. (16) can be rewritten as:

$$\begin{Bmatrix} \cos\omega T \\ \sin\omega T \end{Bmatrix} = \begin{bmatrix} A_{11} & A_{12} \\ A_{21} & A_{22} \end{bmatrix}^{-1} \begin{Bmatrix} B_1 \\ B_2 \end{Bmatrix} = \begin{Bmatrix} C_1 \\ C_2 \end{Bmatrix}, \tag{17a,b}$$

where C_1 and C_2 are computed in terms of the constants A_{ij} and B_i for $i,j = 1,2$.

Squaring and adding Eqs. (17a) and (17b) yields

$$C_1^2 + C_2^2 = 1. \tag{18}$$

Dividing Eq. (17a) by Eq. (17b), yields

$$\tan(\omega T) = \frac{C_2}{C_1}. \tag{19}$$

Simplifying Eq. (18), one obtains the polynomial equation of ω

$$\alpha_1\omega^4 + \alpha_2\omega^2 + \alpha_3 = 0, \tag{20}$$

where $\alpha_1 = 1 - (R + k_c)^2$, $\alpha_2 = (c_e - 2)(1 - R^2) + 2k_cR$, $\alpha_3 = 1 - R^2$.

Eq. (20) has nonnegative real solutions (ω_c) for different values of the control parameters. The corresponding values of the critical time-delay (T_c) on the switching boundary are computed from Eq. (19) as

$$T_c = \frac{1}{\omega_c}\left[\tan^{-1}\left(\frac{C_2}{C_1}\right) + 2i\pi\right], \quad \forall i = 0, 1, 2, \ldots, \infty. \tag{21}$$

It may be noted that the uncontrolled system has a pair of complex conjugate eigenvalues with positive real parts. Thus for the stability of the equilibrium to switch at the critical values computed above, the eigenvalues must cross the imaginary axis from the left half s-plane to the right half s-plane or the vice versa. This is possible when the speed of the crossing with respect to the increasing value of the time-delay is non-trivial. The speed of the crossing of eigenvalues on a switching boundary is expressed as

$$V(\omega_c, T_c) = \text{sign}\left[\text{Re}\left(\frac{ds}{dT}\Big|_{j\omega_c, T_c}\right)\right], \tag{22}$$

where

$$\frac{ds}{dT} = \frac{(Ls^3 - c_eRs^2 + Rs)\,e^{-sT}}{c_e - 2s - \{T(Ls^2 - c_eRs + R) + (c_eR - 2Ls)\}\,e^{-sT}}.$$

The stability characteristic of the equilibrium switches from unstable to stable if $V<0$ and from stable to unstable if $V>0$ when T increases past T_c. Since $V = 0$ signifies non-crossing of the imaginary axis by the eigenvalues, the corresponding critical values must be neglected for the computation of the stability boundaries.

Before proceeding further, it may be noted the system under consideration is a neutral time-delay system. Therefore, it is important to know the behaviour of the non-system poles as T goes for 0 to 0^+. This is checked by the continuity of the roots of the characteristic equation at $T = 0$. For the present problem, the root continuity at $T = 0$ is guaranteed by the stability of the following system:

$$1 - (R + k_c)\,e^{-sT} = 0. \tag{23}$$

It is not difficult to show (see Appendix A) that the system (23) is stable for

$$|R + k_c| < 1. \tag{24}$$

Therefore, stability for any value of the time-delay cannot be achieved when the condition (24) is violated because under this circumstance, the system has infinite number of unstable poles at $T = 0^+$. However, within the range of the gains as prescribed by the condition (24), the number of unstable pair of complex poles at $T = 0^+$ is one.

Using Eqs. (21)–(24), the local stability boundaries in the lowest possible range of delays are computed and the corresponding boundaries are delineated in the planes of control parameters. Figs. 3a and b depict the stability regions in k_c vs. T plane. It is observed that the stability region spreads out in size with the increasing value of the positive recursive gain. With the increasing value of the recursive gain, the stability region extends both way along the gain axis and shifts towards the smaller delay region. Fig. 4 depicts the stability boundaries in R vs. T plane. Fig. 5 depicts the stability plots for different values of the recursive gain and the effective damping c_e. It is observed that the region of stability gradually shrinks with the increasing value of the effective damping c_e. However, higher recursive gains can accommodate larger values of c_e. Thus, the robustness of the control increases with the positive recursive gain. A rigorous discussion on the robustness of the control will be found elsewhere in the paper. An empirical upper bound of the value of c_e for which the system can be

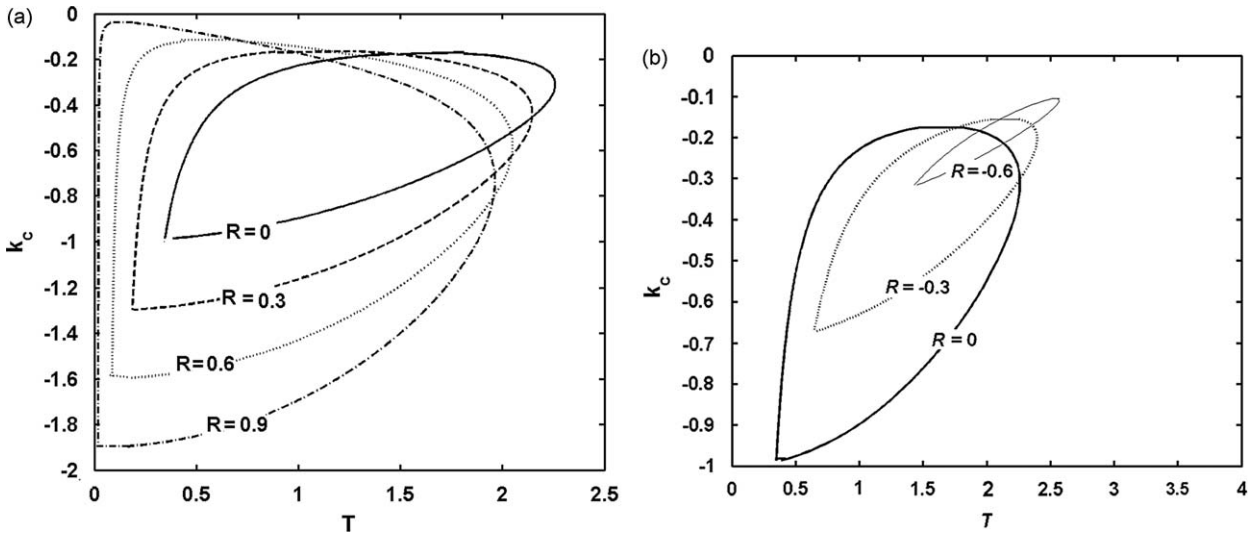

Fig. 3. (a) Regions of local stability of the equilibrium for the acceleration feedback with positive recursive gain. $c_e = 0.1721$. (b) Regions of local stability of the equilibrium for the acceleration feedback with negative recursive gain. $c_e = 0.1721$.

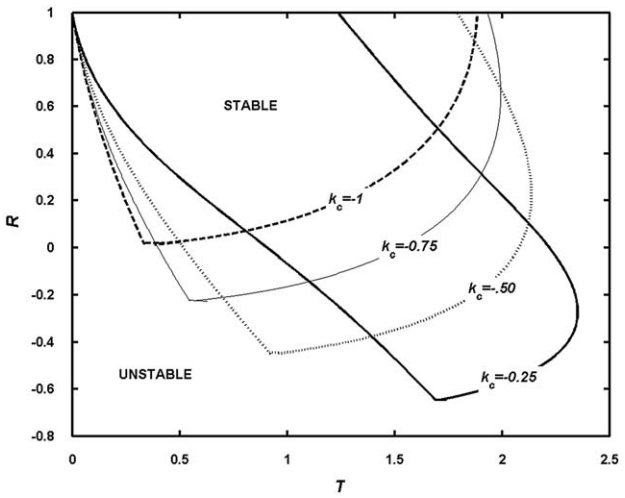

Fig. 4. Regions of local stability of the equilibrium in R vs. T plane. $c_e = 0.1721$.

stabilized by the proposed control action is given as

$$(c_e)^2_{\max} < \frac{1}{2}\left(\frac{1+3R}{1-R}\right). \tag{25}$$

It may be mentioned here that the system is also stable for $R = 1$ (the upper bound of the recursive gain). The characteristics of the system at $R = 1$ is very interesting and calls for a special attention. A separate section will be devoted to discuss this special case.

From the foregoing analysis, it may be inferred that the recursive gain has a significant effect on the stability characteristics of the system. It is already understood that the extent of the stability region in the plane of the control parameters can be modified nontrivially by changing the recursive gain R. A nonlinear analysis presented below will further reveal significant contributions of the recursive parameter to the performance of the control system.

4. Multiple time scale analysis

In the previous section, it is shown that the time-delay feedback can stabilize the unstable equilibrium of a friction-driven system. The local stability boundaries are plotted for different parameter values. However, no clue whatsoever pertaining to the optimum selection of the parameters for the best performance of the system is so far available. In order to

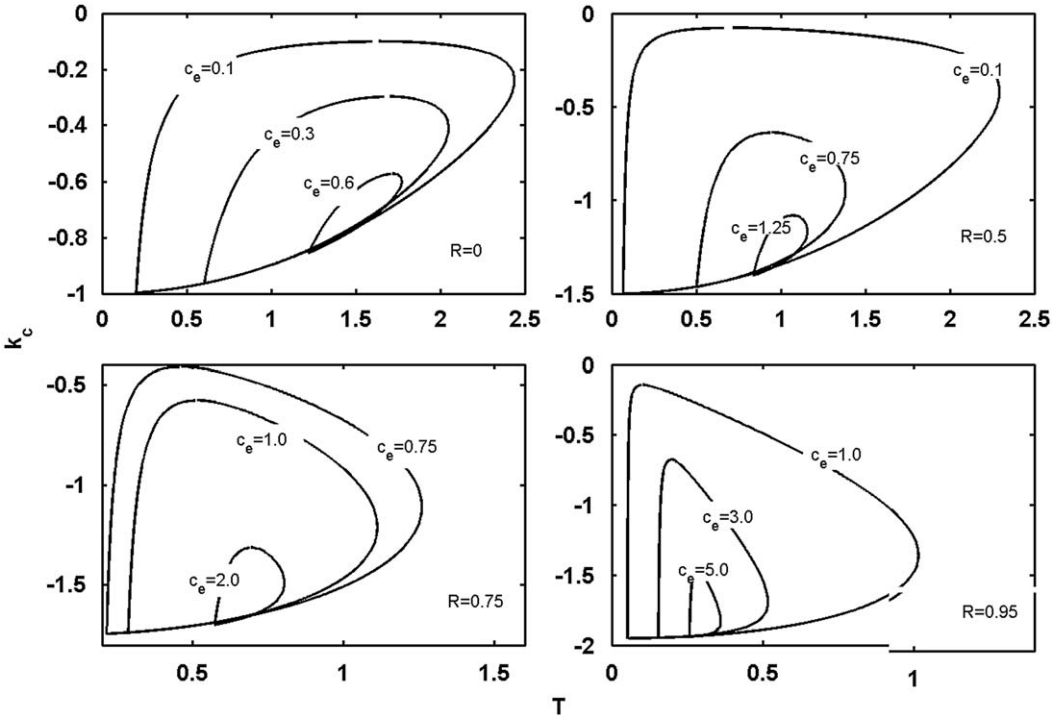

Fig. 5. Stability plots for different values of the recursive gain and the effective damping c_e.

gain a deeper insight into the basic mechanism of the stabilizing effect of the time-delay feedback, a thorough analysis of the system is necessary. Intuitively, the time-delay feedback improves the overall damping of the system. However, an understanding regarding the dependence of the overall damping characteristics of the system on the control parameters is important from the design point of view. Towards this end, a multiple time scale analysis is employed in this section.

For the successful application of the method of multiple time scales, it is assumed that both the inherent nonlinearity of the system as well as the control effort are weak. As before, only the near-equilibrium slipping dynamics is taken into the consternation. Accordingly, Eq. (11) is recast in the following form:

$$\ddot{z} + z = \varepsilon f(\dot{z}) + \varepsilon \tilde{k}_c u, \tag{26}$$

where $k_c = \varepsilon \tilde{k}_c$, $0 < \varepsilon \ll 1$ and $f(\dot{z})$ is written as:

$$f(\dot{z}) = \tilde{\gamma}(e^{a\dot{z}} - 1) - \tilde{c}\dot{z}, \tag{27}$$

where $\gamma = \varepsilon\tilde{\gamma}$ and $c = \varepsilon\tilde{c}$.

The control signal u is expressed as

$$u(\tau) = \sum_{n=1}^{\infty} R^{n-1}\ddot{z}(\tau - nT). \tag{28}$$

The solution of Eq. (26) can be written in the following form:

$$z(\varepsilon, \tau) = z_0(T_0, T_1, \ldots) + \varepsilon z_1(T_0, T_1, \ldots) + \ldots, \tag{29}$$

where $T_n = \varepsilon^n \tau,\ n = 0, 1, 2, \ldots$.

Substituting the expansion (29) into Eqs. (26)–(28) and separating the ε^0 and ε^1 order terms, one obtains

$$D_0^2 z_0 + z_0 = 0, \tag{30}$$

$$D_0^2 z_1 + z_1 = f(\dot{z}_0) - 2D_0 D_1 z_0 + \tilde{k}_c \sum_{n=1}^{\infty} R^{n-1} D_0^2 z_0(\tau - nT), \tag{31}$$

where

$$D_n = \frac{\partial}{\partial T_n}, \quad n = 0, 1, 2, \ldots \quad \text{and} \quad D_i D_j = \frac{\partial}{\partial T_i}\left(\frac{\partial}{\partial T_j}\right).$$

The solution of Eq. (30) is written as

$$z_0 = A(T_1)\sin(T_0 + \Phi(T_1)), \tag{32}$$

where $A(T_1)$ is the amplitude of vibration and $\Phi(T_1)$ is the phase.

Substituting (32) into Eq. (31), yields

$$D_0^2 z_1 + z_1 = f(A\cos\theta) + 2A\frac{\mathrm{d}\Phi}{\mathrm{d}T_1}\sin\theta - 2\frac{\mathrm{d}A}{\mathrm{d}T_1}\cos\theta - \tilde{k}_c A\sum_{n=1}^{\infty} R^{n-1}\sin(\theta - nT), \tag{33}$$

where $\theta = T_0 + \Phi(T_1)$.

The periodic function $f(A\cos\theta)$ can be expanded in the Fourier series as

$$f(A\cos\theta) = a_0 + \sum_{k=1}^{\infty}(a_k\cos(k\theta) + b_k\cos(k\theta)), \tag{34}$$

where

$$a_0(A) = \frac{1}{2\pi}\int_0^{2\pi} f(A\cos\theta)\,\mathrm{d}\theta,$$

$$a_k(A) = \frac{1}{\pi}\int_0^{2\pi} f(A\cos\theta)\cos(k\theta)\,\mathrm{d}\theta,$$

$$b_k(A) = \frac{1}{\pi}\int_0^{2\pi} f(A\cos\theta)\sin(k\theta)\,\mathrm{d}\theta.$$

For the present problem, the single term Fourier expansion of $f(A\cos\theta)$ is

$$f(A\cos\theta) = (2\tilde{\gamma}I_1(aA) - \tilde{c}A)\cos\theta, \tag{35}$$

where $I_1(.)$ is the modified Bessel's function of order one.

Substituting (35) into Eq. (32), yields

$$D_0^2 z_1 + z_1 = \left[2\tilde{\gamma}I_1(aA) - \tilde{c}A - 2\frac{\mathrm{d}A}{\mathrm{d}T_1} + \tilde{k}A\sum_{n=1}^{\infty} R^{n-1}\sin(nT)\right]\cos\theta + \left[2A\frac{\mathrm{d}\Phi}{\mathrm{d}T_1} - \tilde{k}_c A\sum_{n=1}^{\infty} R^{n-1}\cos(nT)\right]\sin\theta \tag{36}$$

Removing the secular terms from Eq. (36) gives the following solvability conditions:

$$2\tilde{\gamma}I_1(aA) - \tilde{c}A - 2\frac{\mathrm{d}A}{\mathrm{d}T_1} + \tilde{k}_c A\sum_{n=1}^{\infty} R^{n-1}\sin(nT) = 0, \tag{37}$$

$$2A\frac{\mathrm{d}\Phi}{\mathrm{d}T_1} - \tilde{k}_c A\sum_{n=1}^{\infty} R^{n-1}\cos(nT) = 0. \tag{38}$$

From Eqs. (37) and (38) one obtains the slow flow equations for the amplitude and phase as

$$\frac{\mathrm{d}A}{\mathrm{d}\tau} = \frac{1}{2}\left[2\gamma I_1(aA) - cA + k_c A S(R,T)\right], \tag{39}$$

$$\frac{\mathrm{d}\Phi}{\mathrm{d}\tau} = \frac{1}{2}k_c C(R,T), \tag{40}$$

where $S(R,T) = \sum_{n=1}^{\infty} R^{n-1}\sin(nT)$ and $C(R,T) = \sum_{n=1}^{\infty} R^{n-1}\cos(nT)$.

It is not difficult to show that (see Appendix B for details)

$$S(R,T) = \frac{\sin(T)}{(1+R^2) - 2R\cos(T)}, \tag{41}$$

and

$$C(R,T) = \frac{\cos(T) - R}{(1+R^2) - 2R\cos(T)}. \tag{42}$$

Linearizing the amplitude equation (Eq. (39)) around the trivial equilibrium, one obtains

$$\frac{\mathrm{d}A}{\mathrm{d}\tau} = \frac{1}{2}[(\gamma a - c) + k_c S(R,T)]A. \tag{43}$$

From Eq. (43) one can obtain the following expression of a measure of the dissipation of the system

$$d = d_s + d_c = -\tfrac{1}{2}(\gamma a - c) - \tfrac{1}{2}k_c S(R,T). \tag{44}$$

Thus, the trivial equilibrium of the system is stable when d is positive. It may be noted that larger the value of d, more is the overall damping of the system. As the system damping d_s is negative, the damping d_c provided by the controller must be sufficiently positive such that overall damping $d>0$. It is noteworthy that the function $S(R,T)$ is periodic in T. However, the multiple time scale analysis seems accurate only for some smaller values of the time-delay. Therefore, in the subsequent discussions the time-delay is assumed to be restricted within the lowest possible range of values. From Eq. (44) it is understood that d_c can be maximized within the stable region of operation by increasing the negative feedback control gain k_c and maximizing $S(R,T)$, which in turn depends on the recursive gain R and the time-delay T. Understanding the dependence of the functions $S(R, T)$ on R and T is, therefore, important.

From the expression of $S(R,T)$ given in Eq. (41) it is easy to show that for a chosen value of the delay, the maximum value of S is

$$\max_R\{S(R,T)\} = \frac{1}{\sin(T)} \quad \text{for } R = \cos T. \tag{45}$$

On the other hand, for a chosen value of the recursive gain R, the maximum value of S is

$$\max_T\{S(R,T)\} = \frac{1}{1-R^2} \quad \text{for } T = \cos^{-1}\left(\frac{2R}{1+R^2}\right). \tag{46}$$

From the expressions (45) and (46) it is now clear that $S(R,T)$ can be increased by choosing either R close to unity ($|R|<1$) and small time-delay or R close to -1 and the time-delay close to π. However, the second choice is infeasible because of the system is unstable for this combination of values as evident from the stability plots depicted in Figs. 3–4. The variations of $S(R,T)$ with T for different values of R shown in Fig. 6 substantiate the above observations. However due to hardware constraints, using a very small value of the time-delay may be impractical. Under these circumstances, one should select the minimum possible time-delay and the corresponding best value of the recursive gain R as computed from Eq. (45).

From the expression (41) it is clear that for the ordinary time-delay feedback (which corresponds to the case $R=0$), the maximum value of S is unity and the corresponding time-delay is $\pi/2$. However, it is possible to increase the value of S far beyond unity and theoretically to infinity by the recursive feedback, i.e., for a nontrivial positive value of R. Thus, the recursive delay feedback can significantly improve the overall damping of the system.

Before proceeding further, it will not be out of place to comment a line or two on the nonlinear stability characteristics of the trivial equilibrium. Towards this end, the amplitude equation (Eq. (39)) is recast in the following form after expanding the modified Bessel's function into the Taylor series around $A=0$:

$$\frac{dA}{d\tau} = -dA + \frac{1}{16}\gamma a^3 A^3 + O(A^5). \tag{47}$$

The trivial equilibrium of the amplitude equation (Eq. (47)) undergoes a Hopf bifurcation at $d=0$ and as the coefficient of the cubic term is positive, the bifurcation is subcritical following which the trivial equilibrium becomes stable and an unstable limit cycle emerges. Therefore, the local stability of the equilibrium does not guarantee the amplitude death of the friction-driven, stable limit cycle oscillation. A stable limit cycle can coexist with the stable equilibrium and these two stable solutions are separated by an unstable limit cycle. Thus, the locally stable equilibrium is not necessarily globally stable. Therefore, a global stability analysis is warranted.

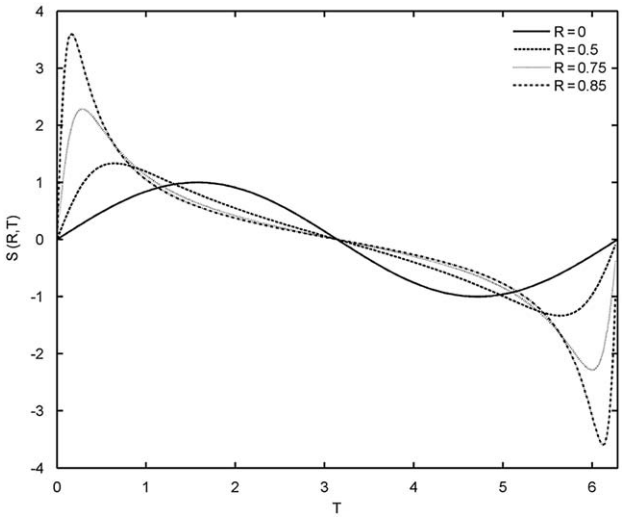

Fig. 6. Variations of $S(R,T)$ with T.

5. Robustness analysis

The exact location and the extent of the region of stability in the plane of the control parameters is sensitive to the value of the effective negative damping c_e . It is already observed in Section 3 that the region of stability gradually shrinks with the increasing value of the effective negative damping generated due to the friction. However in practice, an accurate estimation of the parameter c_e is highly improbable. Thus, it is pertinent to estimate the bound on the variation of the parameter c_e above the nominal that the controlled system can tolerate without loosing its stability. The minimum perturbation of the parameter c_e that the system can endure (before losing stability) is the measure of the robustness of the control. In principle, appropriate choices of the control and the design parameters maximize the robustness. The basic philosophy of estimating the robustness is briefly outlined below.

A negatively damped mechanical oscillator mathematically represents the near-equilibrium dynamics of the uncontrolled system. When the control force is added, the overall damping of the system turns positive and thus, the equilibrium of the controlled system becomes stable. Now the stable control system is again brought on the verge of instability by perturbing the effective damping of the original uncontrolled system by an amount, say p. Then p is the measure of the robustness of the controlled system. In what follows, analytical expressions relating the quantity p with the different control parameters are derived. The optimum characteristics of the robustness of the control are also discussed.

Let p be the perturbation (positive) of the effective damping that will just destabilize the system, which is already stabilized by the feedback. Then one writes the characteristic equation of the system as

$$(s^2 - (c_e + p)s + 1) - ((R + k_c)s^2 - (c_e + p)Rs + R)\,\mathrm{e}^{-sT} = 0. \tag{48}$$

It is known that on the stability boundary the system is marginally stable, i.e., $s = j\omega$. Substituting $s = j\omega$ into Eq. (48) and separating the real and imaginary parts, one obtains the following two equations after some algebraic manipulations:

$$\cos\,\omega T = \frac{1 - \omega^2 - R(R\omega^2 - R + \omega^2 k_c)}{2R - 2R\omega^2 - k_c\omega^2} = f(\omega), \tag{49}$$

and

$$p = \frac{-c_e\omega - (R(\omega^2 - 1) + \omega^2 k_c)\sin\,\omega T + c_e\omega R\cos\,\omega T}{\omega(1 - R\cos\,\omega T)} = h(\omega, T). \tag{50}$$

For maximizing the quantity p with respect to the time-delay T, one requires

$$\frac{\mathrm{d}p}{\mathrm{d}T} = \frac{\partial h}{\partial T} + \frac{\partial h}{\partial \omega}\frac{\mathrm{d}\omega}{\mathrm{d}T} = 0. \tag{51}$$

From Eq. (49), one obtains

$$\frac{\mathrm{d}\omega}{\mathrm{d}T} = -\frac{\omega\,\sin\,\omega T}{T\,\sin\,\omega T + \frac{\mathrm{d}f}{\mathrm{d}\omega}} \tag{52}$$

Substituting Eq. (52) into Eq. (51) and using Eq. (49), one finally obtains the following expression of $\omega = \omega_m$ for which p assumes the maximum value:

$$\omega_m = \left(\frac{1 - R^2}{1 - (R + k_c)^2}\right)^{1/4}. \tag{53}$$

The corresponding time-delay $T = T_m$ is expressed as

$$T_m = \frac{1}{\omega_m}\cos^{-1}\{f(\omega_m)\}. \tag{54}$$

Fig. 7 shows the variations of the optimum value of the time-delay (T_m) and the maximum robustness with the recursive gain for different values of the control gain. The plots are presented in the stable region of operation. It may be observed from the plots presented in Fig. 7 that the maximum robustness increases and the corresponding optimum time-delay decreases with the increasing value of R. Interestingly, the maximum value of the robustness is theoretically infinity for $R = 1$. These results are qualitatively equivalent to the results discussed in the Section 4 where it is shown that the effective damping of the control system increases with R approaching unity and the time-delay approaching the corresponding optimal value. However, the most important observation that may be made from these plots is that the recursive gain has relatively stronger influence on the robustness than the control gain. Further to this, the stability plots shown in Figs. 3–5 confirm that a higher control gain can be used with a higher value of the recursive gain (positive). Thus, the combined effects of these two enhance the maximum achievable robustness. These results clearly confirm the usefulness of the recursive feedback.

The variations of the robustness p with the time-delay for different values of R are plotted in Fig. 8. For the given values of the control parameters, first Eq. (49) is solved for ω and then p is computed from Eq. (50). Due to the transcendental nature of Eq. (49), multiple solutions of ω and p are theoretically possible. However, out of all possible positive values of p

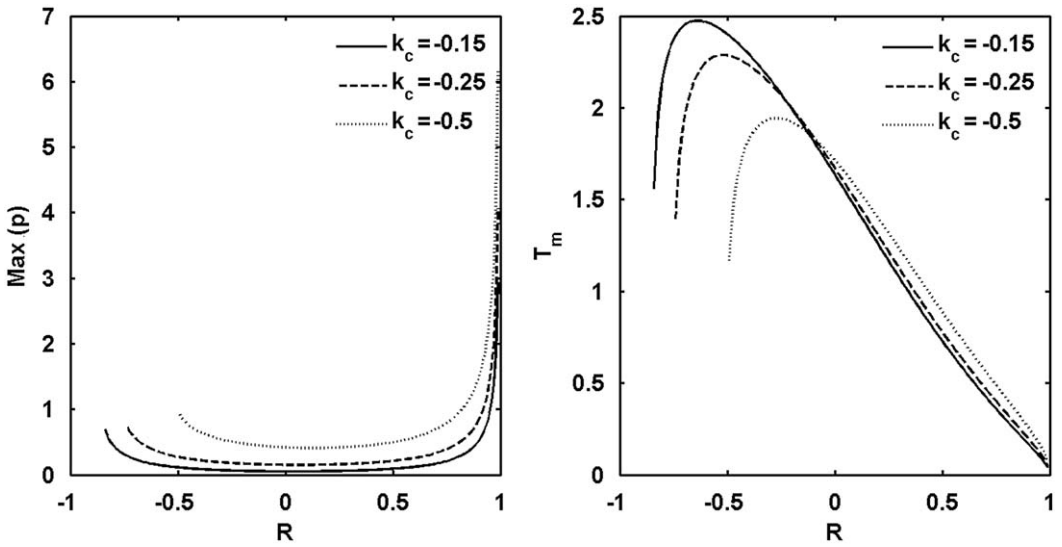

Fig. 7. Variations of (a) the maximum robustness and (b) the optimum time-delay with the recursive gain. $c_e = 0.1$.

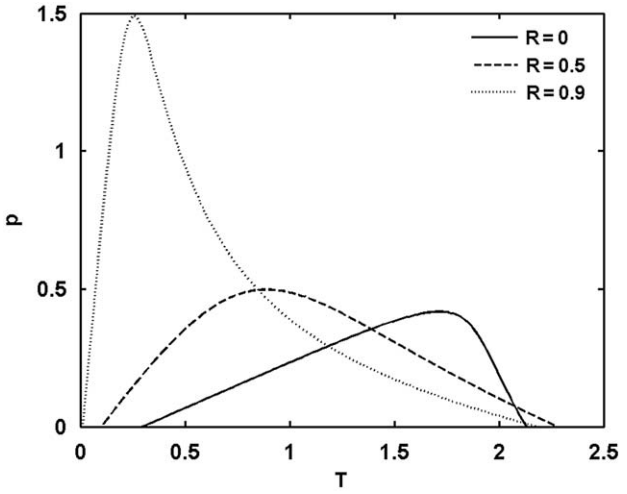

Fig. 8. Variation of robustness p with time-delay. $c_e = 0.1$ and $k_c = -0.5$.

inside the stable region, the minimum value qualifies as the measure of the robustness. Fortunately, Eq. (49) does not have multiple solutions within the range of parameter values studied. The similarity between the plots in Fig. 8 and the plots of $S(R,T)$ vs. T shown in Fig. 6 is a direct evidence of the qualitative concurrence between the results of the Section 4 and that of the present section.

Fig. 9 shows the maps of the robustness measure in the gain vs. delay plane for the recursive and non-recursive, acceleration feedback control. A comparison between these two cases clearly demonstrates that the recursive acceleration feedback is more robust than the non-recursive feedback.

6. System characteristics at $R = 1$

The Laplace transformation of Eq. (14) gives the controller transfer function as

$$G_c(s) = \frac{U(s)}{Z(s)} = \frac{s^2}{1 - \mathrm{Re}^{-sT}}. \tag{55}$$

It is already established that the system is sufficiently stable for smaller values of the time-delay and higher values of the recursive gain. Under these circumstances, one can substitute the exponential function in Eq. (55) with its first order pade

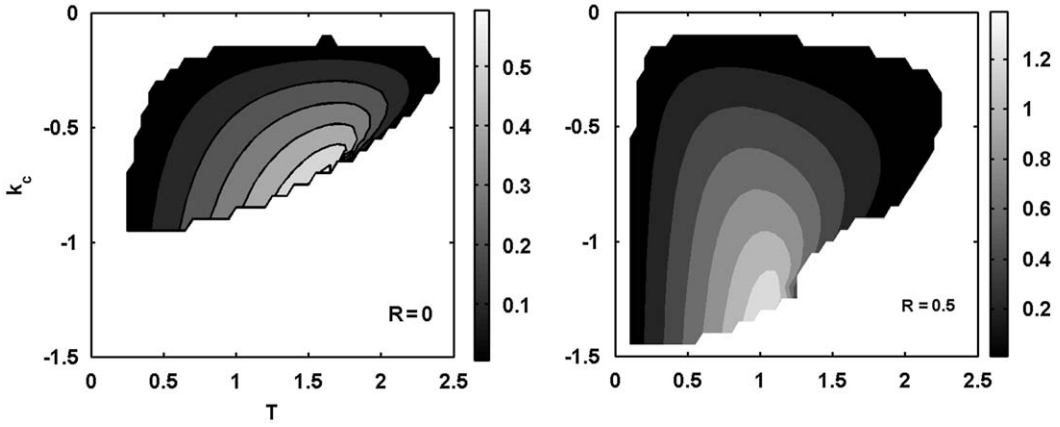

Fig. 9. Robustness map. $c_e = 0.1$.

approximant given as

$$e^{-sT} = \frac{2 - sT}{2 + sT}. \tag{56}$$

Substituting Eq. (56) into (55), yields the following expression of controller transfer function

$$G_c(s) = \frac{U(s)}{Z(s)} = \frac{s^2(2 + sT)}{2(1 - R) + (1 + R)sT}. \tag{57}$$

Taking the Laplace transform of Eq. (14) and using (57), yields the following third order characteristic equation:

$$\lambda_3 s^3 + \lambda_2 s^2 + \lambda_1 s + \lambda_0 = 0, \tag{58}$$

where

$$\lambda_3 = (1 + R - k_c)T, \;\; \lambda_2 = 2(1 - R - k_c) - c_e(1 + R)T, \;\; \lambda_1 = (1 + R)T - 2c_e(1 - R), \;\; \text{and} \;\; \lambda_0 = 2(1 - R)$$

Now it is easy to see from Eqs. (55) and (58) that one pole of the system becomes zero at $R = 1$. However, it is also apparent from Eq. (57) that there is a pole-zero cancellation in the controller transfer function at $s = 0$; this reduces the effective order of the system by one. For $R = 1$, Eq. (57) is rewritten as

$$G_c(s) = \frac{U(s)}{Z(s)} = \frac{s(2 + sT)}{2T}. \tag{59}$$

Taking the Laplace transform of Eq. (15) and using (59), yields the following second order characteristic equation:

$$s^2 - \frac{\left(c_e + \dfrac{k_c}{T}\right)}{\left(1 - \dfrac{k_c}{2}\right)} s + \frac{1}{\left(1 - \dfrac{k_c}{2}\right)} = 0. \tag{60}$$

In light of the above discussions, the region of stability of the system for $R = 1$ can now be obtained by the method described in Section 3. Actually, the above method gives the region of marginal stability because there always exists a pole at the origin. However, as this pole is actually cancelled by a zero of the controller, the marginally stable region obtained by the above method is actually the stable region. The regions of stability for $R = 1$ are shown in Fig. 10. Clearly, the lower threshold of the time-delay for the stable operation is $T = 0^+$. Thus, the system can be stabilized for an infinitesimally small value of the time-delay.

The approximate second order system described by Eq. (60) elucidates the qualitative characteristics of the system at $R = 1$. It is apparent from the coefficient of the s term of Eq. (60) that the degree of stability improves with the decreasing value of the time-delay. In fact, the degree of stability is inversely proportional to the time-delay. The degree of stability as well as the damping improves with the gain. However, the natural frequency of the system remains independent of the time-delay. However, the above analysis seems to be valid only for small values of the control gain.

7. Numerical results and discussions

This section presents some numerical evidences in favour of the analytical results obtained in Sections 4–6. First the variations of the damping and the natural frequencies of the dominant poles of the linearized system are studied. Then

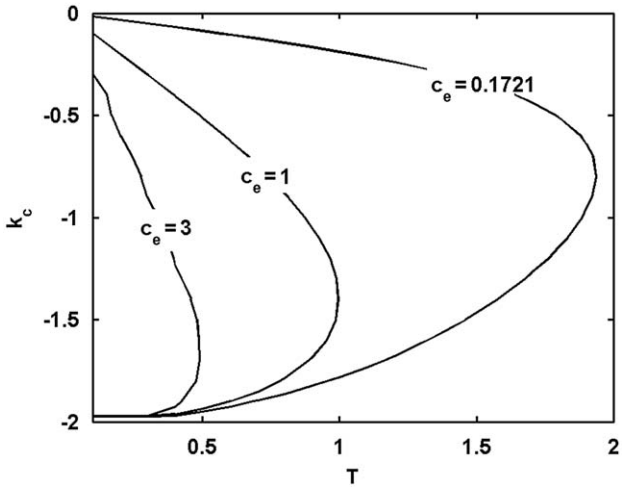

Fig. 10. Stability plots for $R = 1$.

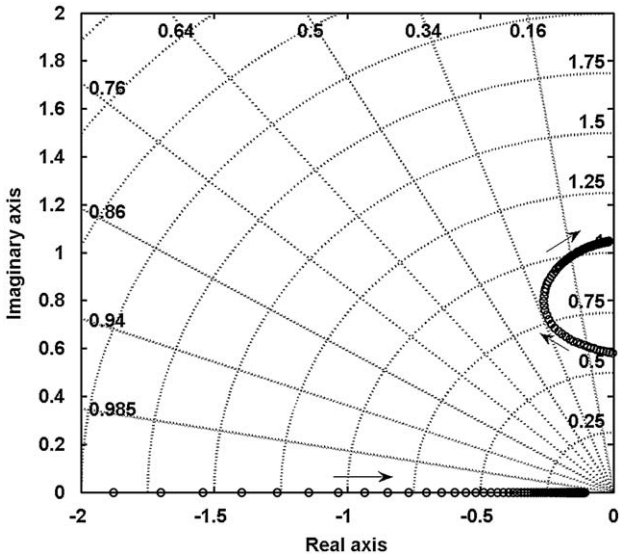

Fig. 11. Movement of the dominant poles in the complex plane with the time-delay. T is varied up to 1. Arrows indicate the direction of the movement of the poles with the increasing value of the time-delay. $c_e = 0.1721$, $R = 0.9$, $k_c = -0.2$.

numerical simulations of the nonlinear system equations are carried out to demonstrate the efficacy of the proposed control method.

7.1. Damping factor and natural frequency

In Section 4, the variations of the damping and the frequency of oscillations with the time-delay have been discussed. However, the results are valid only for smaller gains. In this section, the damping and natural frequencies of the dominant poles of the system are directly computed and hence the results of the Section 4 are extended also to higher gains. The poles of the system are computed using the *quasi-polynomial mapping algorithm* given in [28]. The movements of the dominant poles, the associated damping factors and the natural frequencies with the increasing time-delay are shown in Figs. 11–14. The corresponding values are listed in Tables 1–4. Characteristic behaviour of the dominant poles of the system for different values of the control and the recursive gain are discussed below for a specific value of c_e (here 0.1721 that corresponds to the values of the friction model parameters listed in Table 5).

Case 1: $R < 1$, low gain

For a small gain, a pair of dominant complex pole first reaches a high damping region and then drifts away to a low damping region. However, the natural frequency of the complex poles gradually increases with the increasing value of the

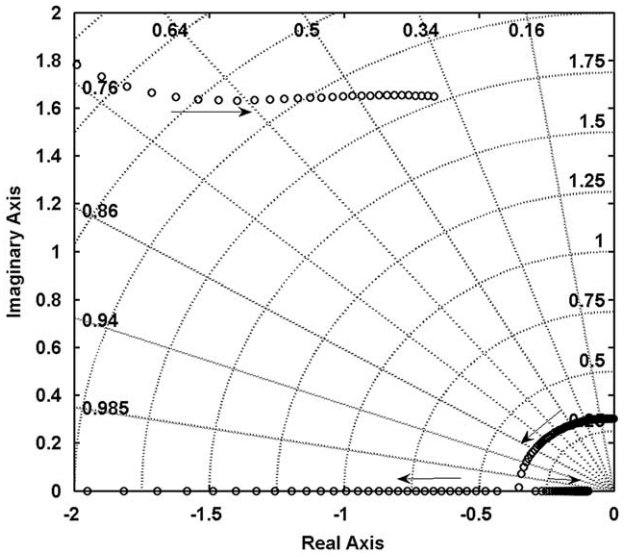

Fig. 12. Movement of the dominant poles in the complex plane with the time-delay. T is varied up to 1.2. Arrows indicate the direction of the movement of the poles with the increasing value of the time-delay. $c_e = 0.1721$, $R = 0.9$, $k_c = -1$.

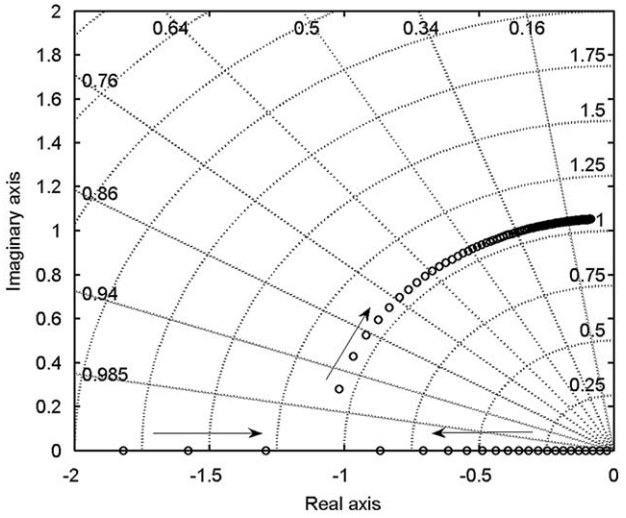

Fig. 13. Movement of the dominant poles in the complex plane with the time-delay. T is varied up to 0.6. Arrows indicate the direction of the movement of the poles with the increasing value of the time-delay. $c_e = 0.1721$, $R = 1$, $k_c = -0.2$.

time-delay. Simultaneously a real pole moves towards the dominant complex poles with the increasing value of the time-delay, but never goes to the right of the dominant complex pole. Thus, it may be concluded that when R is less than unity and the control gain is small, the damping gradually increases to the maximum value and again decreases with the increasing value of the time-delay. For this case, the movement of the dominant poles in the complex plane is depicted in Fig. 11 and the corresponding values are tabulated in Table 1.

Case 2: $R < 1$, high gain

For a large control gain, a pair of dominant complex poles initially goes towards the higher damping region with the increasing value of the time-delay and eventually the complex poles disappear giving rise to two dominant real poles, one moving towards the left and the other towards the imaginary axis. However, a pair of high-frequency complex poles gradually gains strength with the increasing value of the delay. Thus, the system response remains under-damped for smaller values of the delay and the damping gradually increases to the maximum value and again decreases with the increasing value of the time-delay. However, as the real pole goes to the right of the complex poles, the system response for higher values of the time-delay becomes sluggish and appears to be over-damped. The natural frequency is much less than

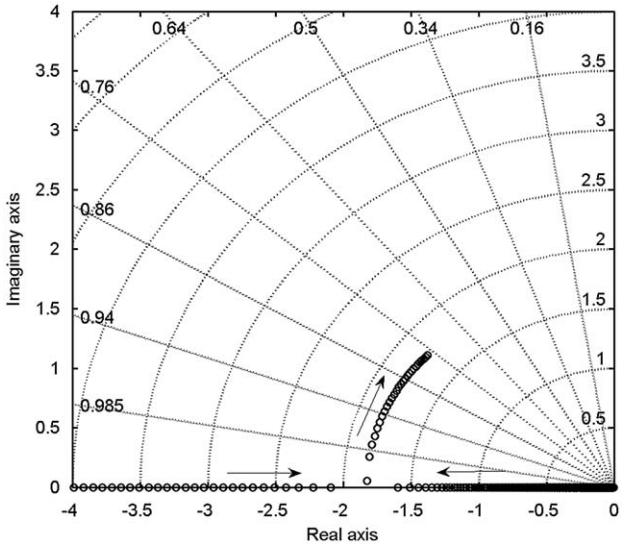

Fig. 14. Movement of the dominant poles in the complex plane with the time-delay. T is varied up to 0.8. Arrows indicate the direction of the movement of the poles with the increasing value of the time-delay. $c_e = 0.1721$, $R = 1$, $k_c = -1$.

Table 1
$c_e = 0.1721$, $R = 0.9$, $k_c = -0.2$.

Time-delay	$T = 0.05$	$T = 0.1$	$T = 0.2$	$T = 0.3$	$T = 0.4$	$T = 0.5$	$T = 0.7$
Dominant	−0.03+0.58i	−0.08+0.60i	−0.22+0.68i	−0.25+0.86i	−0.18+0.95i	−0.13+1.00i	−0.07+1.03i
Poles	−6.88	−3.19	−1.14	−0.48	−0.31	−0.23	−0.15
Damping factor	0.05	0.13	0.3	0.28	0.18	0.12	0.06
Natural frequency	0.58	0.6	0.71	0.89	0.96	1.01	1.03

Table 2
$c_e = 0.1721$, $R = 0.9$, $k_c = -1$.

Time-delay	$T = 0.05$	$T = 0.3$	$T = 0.4$	$T = 0.5$	$T = 0.7$	$T = 0.9$	$T = 1.2$
Dominant	−0.01+0.30i	−0.12+0.28i	−0.17+0.26i	−0.23+0.23i	−0.22	−0.14	−0.09
Poles					−0.57	−1.48	0.66+1.64i
Damping factor	0.063	0.4	0.55	0.72	1.11	1.77	0.3749
Natural frequency	0.2	0.31	0.32	0.33	0.36	0.45	1.78

Table 3
$c_e = 0.1721$, $R = 1$, $k_c = -0.2$.

Time-delay	$T = 0.05$	$T = 0.1$	$T = 0.2$	$T = 0.3$	$T = 0.4$	$T = 0.5$
Dominant	−0.28	−1.01+0.28i	−0.45+0.95i	−0.27+1.01i	−0.17+1.04i	−0.12+1.04i
Poles	−3.98					
Damping factor	2.01	0.96	0.43	0.26	0.1613	0.11
Natural frequency	1.05	1.05	1.05	1.05	1.05	1.05

that of the uncontrolled system and increases with the time-delay, particularly in the lower delay region. For this case, the movement of the dominant poles in the complex plane is depicted in Fig. 12 and the corresponding values are tabulated in Table 2.

Case 3: $R = 1$, low gain

Table 4
$c_e = 0.1721$, $R = 1$, $k_c = -1$

Time-delay	$T = 0.05$	$T = 0.1$	$T = 0.2$	$T = 0.3$	$T = 0.4$	$T = 0.5$	$T = 0.6$	$T = 0.7$
Dominant Pole(s)	−0.05	−0.1	−0.21	−0.3336	−0.4769	−0.66	−0.93	−1.79+0.36i
	−132.02	−57.11	−23.53	−13.3656	−8.5513	−5.73	−3.78	
Damping factor	25.7	11.97	5.34	3.26	2.25	1.64	1.25	0.98
Natural frequency	2.57	2.39	2.22	2.09	2.0	1.94	1.87	1.82

Table 5
Parameter values of the friction model used for numerical simulations.

Parameter	Numerical value	Remark
μ	0.2	Friction model parameters
$\Delta\mu$	0.2	$c_e = 0.1721$
a	1.0	
v_0	0.15	
c	0.0	

The dominant poles are real for smaller time-delays and hence the system response is over-damped and sluggish. With the increasing value of the delay, the most dominant real pole moves away and the other moves towards the imaginary axis before being coalesced into a pair of dominant complex poles. Thus, the system response becomes under-damped beyond a particular value of the time-delay. For small gains, the natural frequency appears to have no dependence on the time-delay and very close to that of the uncontrolled system. For this case, the movement of the dominant poles in the complex plane is depicted in Fig. 13 and the corresponding numerical values are tabulated in Table 3.

Case 4: $R = 1$, large gain

The characteristics of the movement of the poles in the complex plane are qualitatively the same as observed in case of the small gain. Thus, the system response is over-damped for smaller delays and under-damped for larger delays. However, the critical delay after which the response becomes under-damped is higher in case of larger gain. The natural frequency is higher than that of the uncontrolled system. The natural frequency of the over-damped system decreases with the increasing value of the time-delay, but that of the under-damped response remains almost independent of the time-delay. For this case, the movement of the dominant poles in the complex plane is depicted in Fig. 14 and the corresponding numerical values are tabulated in Table 4.

7.2. Numerical simulations

The stability analysis discussed hitherto only addresses the local stability of the equilibrium of the system. It is already mentioned in Section 4 that the Hopf bifurcation taking place on the stability boundary is subcritical in nature. This implies that stable limit cycle oscillations may coexist with the stable equilibrium even inside the local stability region, particularly near the stability boundary. The desired global stability of the equilibrium is thus not implied by the local stability. Therefore, direct numerical simulations of the mathematical model of the system are employed to investigate the global stability of the equilibrium. Moreover, this section also substantiates some of the major analytical results of the present article. Towards this end, a MATLAB SIMULINK model of the system is developed based on Eqs. (6)–(10). Simulations are carried out for the system parameters given in Table 5.

In order to demonstrate the global stability of the system, numerical simulations are carried out from different initial conditions. The control parameters are chosen inside the local stability boundary as denoted by the point P in Fig. 15. The corresponding damping factor is 0.72 as read from Table 2. Fig. 16 shows the results of numerical simulations in the phase-plane. The trajectories starting from different initial conditions converge to the equilibrium; this confirms the global stability of the equilibrium.

Figs. 17 and 18 depict the numerically simulated time history plot of the oscillator displacement for different values of T. It is observed that the damping of the system with $R = 0.9$ (<1) first increases with the time-delay and eventually the system response becomes over-damped. However, beyond a particular value of the time-delay again under-damped transient oscillation is observed. However, for $R = 1$, the system response is over-damped in the lower delay region, and the response gradually turns under-damped with the increasing value of the time-delay. These results clearly affirm the conclusions reached in earlier sections of the article.

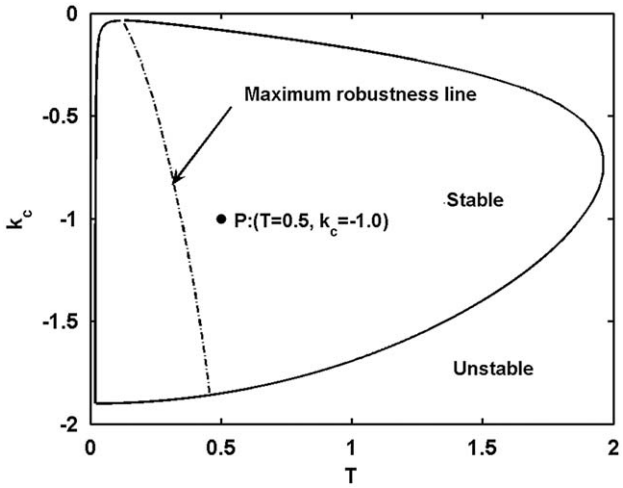

Fig. 15. Control parameter values used for numerical simulation. P denotes the point where numerical simulations are carried out. $R = 0.9$.

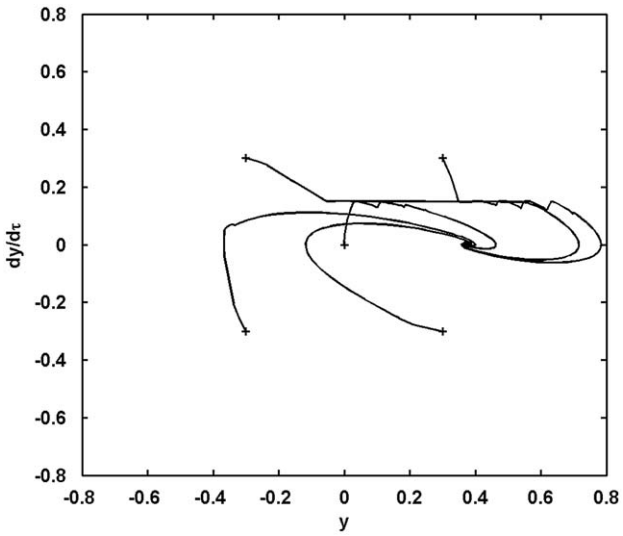

Fig. 16. Phase plots generated by numerical simulations. + signs denote initial points.

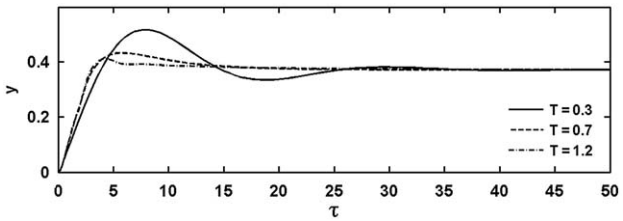

Fig. 17. Time history plots for different values of the time-delay. $R = 0.9$, $k_c = -1$.

7.3. Discussions

The above numerical results are presented for a particular value of the negative effective damping present in the uncontrolled system. However, the results are sufficiently suggestive of the overall qualitative behaviour of the controlled system. The recursive gain can enhance the system damping to any desired value and thus can control any degree of instability inherent in the system. For the recursive gain less than unity, the overall damping first increases to the

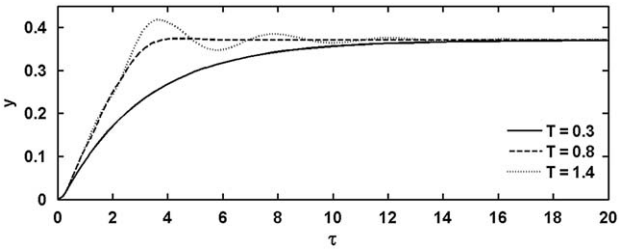

Fig. 18. Time history plots for different values of the time-delay. $R = 1$, $k_c = -1$.

maximum value (may be over-damped depending upon the parameter values) and then decreases with the increasing value of the delay. Whereas, for the unity recursive gain, the system damping is large for smaller values of the delay and decreases with the increasing value of the time-delay. Thus, the conclusions reached in Section 4 for weak control also hold good for stronger control.

8. Conclusions

The present article proposes a novel method of controlling the friction-induced instability by the recursive time-delayed acceleration feedback. A single dof mechanical oscillator on a moving belt represents the basic friction-driven system. The instability inherent in the system is attributed to the velocity-weakening friction characteristic at the belt-mass interface. The control force is synthesized based on an infinite weighted sum of the acceleration of the vibrating mass measured at regular intervals in the past. Such a control signal can also be produced by the recursive summation of the time-delayed acceleration and the time-delayed control signal. The technique is thus termed as the recursive time-delayed acceleration feedback control.

The non-dimensional mathematical model of the system contains three available control parameters, namely the control gain, time-delay and the recursive gain. The degree of instability in the friction-driven system is quantified by a single parameter termed here as the effective negative damping. In case of a trivial recursive gain, the system reduces to an ordinary time-delayed acceleration feedback control that has been previously studied by several researchers. The local stability analysis of the equilibrium of the system is performed and the stability regions are delineated in the planes of the control parameters. It is shown that the recursive feedback can nontrivially modify the stability regions. The stability boundary spreads out both ways along the control gain axis whereas the lower and the upper thresholds of the time-delay shift towards the lower delay regions with the increasing value of the positive recursive gain. A higher value of the recursive gain is required to stabilize an uncontrolled system with a higher degree of instability. An empirical relationship is proposed to estimate the maximum value of the effective negative damping that can be stabilized by a given recursive gain. This clearly establishes the usefulness of the recursive feedback.

A multiple time scale based nonlinear analysis elucidates the role of the recursive gain in enhancing the overall damping effect produced by the control action. It is shown that the overall damping can be increased to any desirable value by increasing the recursive gain and appropriately selecting the time-delay.

The robustness of the control is also discussed. The robustness is defined as the maximum deviation of the effective negative damping produced by the friction force over its nominal value that the control system can accommodate without loosing its stability for a given set of the control parameters. Formula for maximizing the robustness of the control is derived. It is shown that the robustness of the control can be maximized by increasing the control gain and an appropriate value of the time-delay. The robustness increases with the increasing value of the recursive gain. The robustness is shown to assume theoretically infinite value for the unity recursive gain.

A separate section is devoted to analyze the stability of the system for the unity recursive gain. It is shown that for the unity recursive gain, a system pole is placed at the origin but kept silent by a system zero at the origin provided by the controller. Due to the pole-zero cancellation, the effective order of the system is reduced by one. It is also shown that in the limit of small time-delay, the damping produced by the controller varies inversely proportional to the time-delay. Thus, the damping can theoretically reach an infinitely large value for the unity recursive gain.

Numerical results are presented in support of the above observations. The movements of the dominant poles of the system in the complex plane with the increasing value of the time-delay are plotted for four different combinations of the control and the recursive gains. These numerical results confirm that the analytical results for weak control also hold good for stronger control.

The multiple time scale analysis establishes that the Hopf bifurcations taking place on the local stability boundaries are subcritical in nature. Thus, the global stability of the equilibrium is not guaranteed inside the local stability region. In order to analyse the global stability of the equilibrium, the system equations are numerically simulated in MATLAB. For a given set of the system parameters, direct numerical simulations are run from different initial conditions. With the appropriate

choices of the control parameters, the responses starting from different initial conditions are observed to settle down to the equilibrium; this confirms the global stability of the system.

Finally, it may be concluded that an ordinary acceleration feedback control can stabilize only a limited degree of inherent instability, whereas the recursive control offers an all important flexibility to the designer in choosing an appropriate set of robust control parameters for stabilizing almost any degree of instability inherent in the system. Though only a particular example of friction-induced instability has been discussed here, the proposed method is equally applicable to any self-excited system having a significantly large amount of instability that cannot be removed by an ordinary time-delayed feedback.

Appendix A

The condition of the delay-independent stability of the system given by Eq. (23) is worked out here. Substituting $s=\sigma+j\omega$ into Eq. (23) and separating the imaginary and the real parts, yields

$$1-(R+k_c)\,\mathrm{e}^{-\sigma T}\cos\,\omega T=0, \tag{A.1}$$

and

$$(R+k_c)\,\mathrm{e}^{-\sigma T}\sin\,\omega T=0. \tag{A.2}$$

If Eq. (A.2) holds good for any value of T, one can write

$$\omega T=n\pi,\quad \text{for } n=0,1,2,\ldots \tag{A.3}$$

Using Eq. (A.3) in Eq. (A.1), one obtains

$$\mathrm{e}^{\sigma T}=(-1)^n(R+k_c). \tag{A.4}$$

The system is stable when $\sigma<0$, which implies

$$|R+k_c|<1. \tag{A.5}$$

Appendix B

As defined

$$S(R,T)=\sum_{k=1}^{\infty}R^{k-1}\sin(kT), \tag{B.1}$$

and

$$C(R,T)=\sum_{k=1}^{\infty}R^{k-1}\cos(kT). \tag{B.2}$$

Define a complex quantity

$$Z(R,T)=C(R,T)+\mathrm{j}S(R,T)=\sum_{k=1}^{\infty}R^{k-1}\{\cos(kT)+\mathrm{j}\sin(kT)\}=\frac{1}{R}\sum_{k=1}^{\infty}R^k\mathrm{e}^{\mathrm{j}kT}, \tag{B.3}$$

where $\mathrm{j}=\sqrt{-1}$.

Let

$$\eta=R\mathrm{e}^{\mathrm{j}T}. \tag{B.4}$$

Substituting Eq. (B.4) into Eq. (B.3), one obtains for $|R|<1$

$$RZ(R,T)=\sum_{k=1}^{\infty}\eta^k=\frac{\eta}{1-\eta}. \tag{B.5}$$

Equation (B.5) is rewritten as

$$RZ(R,T)[1-\eta]-\eta=0. \tag{B.6}$$

Separating the real and imaginary parts of the left hand side expression of Eq. (B.6), yields

$$\begin{bmatrix} R^2\sin\,T & R(1-R\cos\,T)\\ R(1-R\cos\,T) & -R^2\sin\,T\end{bmatrix}\begin{Bmatrix} S(R,T)\\ C(R,T)\end{Bmatrix}=\begin{Bmatrix} R\cos\,T\\ R\sin\,T\end{Bmatrix}. \tag{B.7}$$

Solving Eq. (B.7) for S and C, one obtains

$$S(R,T) = \frac{\sin T}{1 + R^2 - 2R\cos T} \tag{B.8}$$

and

$$C(R,T) = \frac{\cos T - R}{1 + R^2 - 2R\cos T} \tag{B.9}$$

References

[1] R.A. Ibrahim, Friction-induced vibration, chatter, squeal, and chaos part II: dynamics and modeling, *Transactions of ASME, Applied Mechanics Review* 47 (7) (1994) 227–253.
[2] E.J. Berger, Friction modeling for dynamic system simulation, *Transactions of ASME, Applied Mechanics Review* 55 (6) (2002) 535–577.
[3] M.A. Heckl, D. Abrahams, Active control of friction driven oscillations, *Journal of Sound and Vibration* 193 (1) (1996) 417–426.
[4] K. Popp, M. Rudolph, Vibration control to avoid stick-slip motion, *Journal of Vibration and Control* 10 (2004) 1585–1600.
[5] J.J. Thomsen, Using fast vibrations to quench friction-induced oscillations, *Journal of Sound and Vibration* 228 (5) (1999) 1079–1102.
[6] S. Chatterjee, T.K. Singha, S.K. Karmakar, Effect of high-frequency excitation on a class of mechanical systems with dynamic friction, *Journal of Sound and Vibration* 269 (2004) 61–89.
[7] S. Chatterjee, Non-linear control of friction-induced self-excited vibration, *International Journal of Nonlinear Mechanics* 42 (3) (2007) 459–469.
[8] S. Chatterjee, On the design criteria of dynamic vibration absorbers for controlling friction-induced oscillations, *Journal of Vibration and Control* 14 (3) (2008) 397–415.
[9] A. Maccari, Vibration control for the primary resonance of a cantilever beam by a time delay state feedback, *Journal of Sound and Vibration* 259 (2) (2003) 241–251.
[10] R. Sipahi, N. Olgac, Active vibration suppression with time delayed feedback, *Journal of Vibration and Acoustics—Transactions of ASME* 125 (2003) 384–388.
[11] N. Olgac, B.T. Holm-Hansen, A novel active vibration absorption technique: delayed resonator, *Journal of Sound and Vibration* 176 (1994) 93–104.
[12] J.C. Ji, A.Y.T. Leung, Resonances of a non-linear s.d.o.f. system with two time-delay in linear feedback control, *Journal of Sound and Vibration* 253 (5) (2002) 985–1000.
[13] F.M. Atay, Van der Pol's oscillator under delayed feedback, *Journal of Sound and Vibration* 218 (2) (1998) 333–339.
[14] F.M. Atay, Delayed feedback control of oscillations in nonlinear planar systems, *International Journal of Control* 75 (2002) 297–304.
[15] A. Maccari, Vibration control of parametrically excited Lienard system, *International Journal of Nonlinear Mechanics* 41 (2006) 146–155.
[16] A. Maccari, Vibration control for the primary resonance of a cantilever beam by a time delay state feedback, *Journal of Sound and Vibration* 259 (2) (2003) 241–251.
[17] A. Maccari, Vibration control for the primary resonance of the Van der Pol oscillator by a time delay state feedback, *International Journal of Nonlinear Mechanics* 38 (2003) 123–131.
[18] X. Li, J.C. Ji, C.H. Hansen, C. Tan, Response of a Duffing-Van der Pol oscillator under delayed feedback control, *Journal of Sound and Vibration* 291 (2006) 644–655.
[19] F.-J. Elmer, Controlling friction, *Physical Review E* 57 (1998) 4903–4906.
[20] K. Pyragas, *Physics Letters A* 170 (1992) 421–424.
[21] J. Das, A.K. Mallik, Control of friction driven oscillation by time-delayed state feedback, *Journal of Sound and Vibration* 297 (3–5) (2006) 578–594.
[22] S. Chatterjee, Time-delayed feedback control of friction-induced instability, *International Journal of Nonlinear Mechanics* 42 (2007) 1127–1143.
[23] S. Chatterjee, P. Mahata, Time-delayed absorber for controlling friction-induced self-excited oscillation, *Journal of Sound and Vibration* 322 (2009) 39–59.
[24] J.E.S. Socolar, D.W. Sukow, D.J. Gauthier, Stabilizing unstable periodic orbits in fast dynamical systems, *Physical Review E* 50 (1994) 3245–3248.
[25] S. Chatterjee, Vibration control by recursive time-delayed acceleration feedback, *Journal of Sound and Vibration* 317 (1–2) (2008) 67–90.
[26] N. Hinrichs, M. Oestreich, K. Popp, On the modeling of friction oscillators, *Journal of Sound and Vibration* 216 (3) (1998) 435–459.
[27] R. Horvath, Experimental Investigation of Excited and Self-Excited Vibration, Master's Thesis, University of Technology and Economics, Budapest, 2000. 〈http://www.auburn.edu/~horvaro/index2.htm〉.
[28] T. Vyhlídal, P. Zítek, Quasipolynomial mapping based rootfinder for analysis of time delay systems, *Proceedings of IFAC Workshop on Time-Delay Systems*, TDS'03, Rocquencourt, 2003.